Hindawi Publishing Corporation
ISRN Nanotechnology
Volume 2014, Article ID 867139, 6 pages
http://dx.doi.org/10.1155/2014/867139

Research Article

Structural and Magnetic Properties of Microwave Assisted Sol-Gel Synthesized $La_{0.9}Sr_{0.1}MnO_3$ Manganite Nanoparticles

Mahin Eshraghi[1] and Parviz Kameli[2]

[1] *Department of Physics, Payame Noor University, Tehran 19395-3697, Iran*
[2] *Department of Physics, Isfahan University of Technology, Isfahan 84156-83111, Iran*

Correspondence should be addressed to M. Eshraghi; mahin_eshraghi@yahoo.com

Received 24 November 2013; Accepted 31 December 2013; Published 10 February 2014

Academic Editors: G. F. Goya and L. Suber

The structural and magnetic properties of nanoparticles of $La_{0.9}Sr_{0.1}MnO_3$ (LSMO) were studied using powder X-ray diffraction (XRD), transmission electron microscope (TEM), and magnetic measurements. The XRD refinement result indicates that samples crystallize in the rhombohedral structure with R-3C space group. The dc magnetization measurements revealed that samples exhibit no hysteretic behavior at room temperature, symptomatic of the superparamagnetic (SPM) behavior. The results of ac magnetic susceptibility measurements show that the susceptibility data are not in accordance with the Néel-Brown model for SPM relaxation but fit well with conventional critical slowing down model which indicates that the dipole-dipole interactions are strong enough to cause superspin-glass-like phase in LSMO samples.

1. Introduction

Magnetic nanoparticles are currently the subject of intense research because of their potential applications in high density magnetic storage and biomedical applications [1–3]. The perovskite manganite with the formula $La_{1-x}A_xMnO_3$ (A = Sr, Ca, Ba, or vacancies) has attracted considerable attention due to the discovery of the phenomenon of colossal magnetoresistance (CMR) and its potential application [4–7]. The properties of these materials are explained by double exchange theory of Zener [7] and electron lattice interaction [8]. By varying the composition x and consequently tuning the Mn^{3+}/Mn^{4+} ratio, the compound $La_{1-x}A_xMnO_3$ reveals various electronic, magnetic, and structural phase transitions at different temperatures. These phase transitions have been attributed to strong coupling among spin, charge, orbital degree of freedom, and lattice vibrations.

It is well known that the magnetic and transport properties of these materials strongly depend on the particle size, due to the influence of structural and magnetic disorders at the grain boundaries [9–13]. The size effects and the large surface area of magnetic nanoparticles intensely change some of the magnetic properties compared to bulk counter parts. Manganite nanoparticles display features like lower values of magnetization [14], higher values of low field magnetoresistance [15], exhibiting superparamagnetic (SPM) phenomena [16], and so forth. SPM nanoparticles with single domain microstructure have a high potential as carriers for biomedical applications. According to the Stoner-Wohlfarth theory, the magnetocrystalline anisotropy energy, E_a, of a single-domain particle can be approximated by $E_a = KV \sin 2\theta$, where K is the magnetocrystalline anisotropy constant, V is the volume of the nanoparticle, and θ is the angle between the magnetization direction and the easy axis of the nanoparticle. E_a serves as an energy barrier for blocking the flips of magnetic moments. When E_a becomes comparable with thermal activation energy, K_BT with K_B as the Boltzmann constant, thermal activation can overcome the anisotropy energy barrier. This state occurs above the blocking temperatures, T_B, called SPM state. At blocking temperature, thermal energy is equal to the anisotropy energy. The absence of hysteresis, almost incalculable coercivity

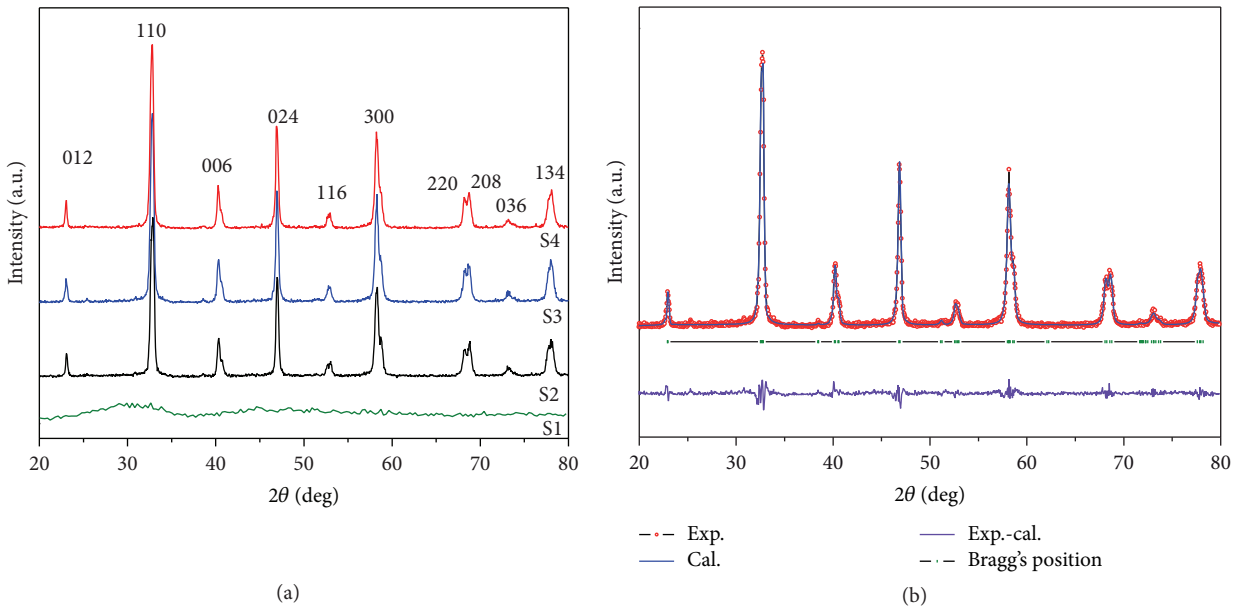

Figure 1: (a) The XRD pattern of S1, S2, S3, and S4 samples at room temperature. (b) The observed and calculated (Rietveld analysis) XRD patterns of S3 sample at room temperature.

and remanence, and the nonachievement of saturation even at high magnetic field are the typical characteristics of SPM behavior [17].

In this paper we have studied the effect of annealing temperature on the structural and magnetic properties of the microwave-assisted sol-gel grown $La_{0.9}Sr_{0.1}MnO_3$ (LSMO) manganite samples.

2. Experimental

The LSMO manganite samples were prepared by the microwave-assisted combustion method using a domestic LG microwave oven operating at frequency of 2.45 GHz with the output power of 1000 W. Stoichiometric amounts of $La(NO_3)_3{\cdot}6H_2O$(Merck, 99%) $n(NO_3)2\cdot 4H_2O$(Merck, 99%) and $Sr(NO_3)$ (Merck, 95%) were dissolved in water and mixed with ethylene glycol and citric acid, forming a stable solution. The mixture was then kept in a microwave oven with 60% of output power. This mixture undergoes dehydration followed by decomposition and spontaneous combustion with the evolution of voluminous gases. The obtained final product is in the form of a foamy powder and is calcined at 450°C (S1) for 6 h. Different packages of powder were sintered at 550°C (S2), 575°C (S3), and 600°C (S4) for 6 h to obtain powders with different particle sizes.

Phase formation and crystal structure of the powders were checked by XRD pattern using Cu Kα radiation source in the 2θ scan range from 20° to 80°. The average particle sizes of the samples were estimated from TEM micrographs. The ac magnetic susceptibility has been measured versus temperature at different frequencies in the selected range of 33–1000 Hz and using a Lake Shore ac susceptometer model 7000. The dc magnetization was carried out as a function of magnetic field at 295 K using a Meghnatis Daghigh Kavir vibrating sample magnetometer (VSM).

3. Results and Discussion

Figure 1 shows the XRD patterns at room temperature for samples. Figure 1(a) shows that S1 sample is amorphous and its crystal structure is not formed. By sintering the powder at higher temperatures, 550°C to 600°C, the perovskite crystal structure is formed. The Rietveld analyses of the XRD pattern of the samples have been carried out using FULLPROF program [18]. Figure 1(b) shows the XRD pattern with Rietveld analysis of the S3 sample. The estimated average lattice parameters are $a = b = 5.511$ Å and c = 13.352 Å which are found in close agreement with reported values [19]. Typically, the TEM micrograph of S3 sample is shown in Figure 2. TEM micrograph shows that the mean particle size of the S3 sample is about 50 nm. Also, the selected area diffraction patterns of sample S3 confirms the crystalline nature of this sample.

To study the magnetic response of samples to an external field, we measured field dependent magnetization using VSM at room temperature. Figure 3 shows the room temperature hysteresis curves of the samples sintered at different temperatures. It can be seen that by increasing the sintering temperature the magnetization (M) increases slightly. An increase in magnetization with the sintering temperature can be attributed mainly due to the enhancement of grain size. The increase of magnetization by increasing the grain size could be ascribed to the lower surface area of larger grains. This is because of the magnetically disordered state in the surface. In the case of nanometric-size grains, defects are expected to occur to a higher extent due to the vacancies, microstrain, and dislocations. Since the sizes of samples

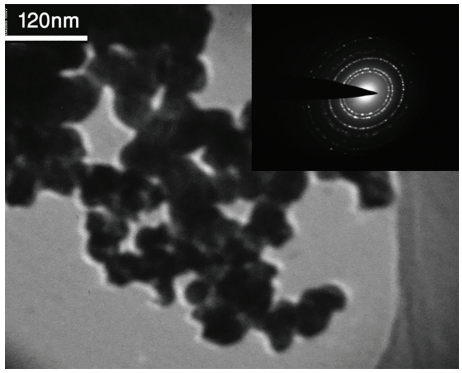

Figure 2: TEM micrograph of sample S3. Upper panel shows the selected area diffraction pattern of sample S3.

are within the superparamagnetic and single domain limits, these samples are SPM in nature with zero coercivity and nonsaturated magnetization.

To further study the SPM behavior of samples, we have performed ac susceptibility measurements on sample S3. Figure 4 shows the real, $\chi'(T)$, and imaginary, $\chi''(T)$, parts of ac magnetic susceptibility as function of temperature in an ac field of 10 Oe and frequencies of 33, 111, 333, 666, and 1000 Hz. It is evident that by decreasing the temperature, the $\chi'(T)$ and $\chi''(T)$ show a peak related to the blocking/freezing temperature (T_B) of the SPM/spin glass systems [20–22]. Above T_B, the nanoparticles considered being in the SPM regime and below which the nanoparticles are in the so-called blocked/freezed regime. T_B is frequency dependent and shifted to higher temperature with increasing frequency. The frequency dependence of the ac magnetic susceptibility is a characteristic of SPM/spin glass systems. There are several models to interpret the ac susceptibility behavior of the magnetic nanoparticles. In the noninteracting SPM system, the frequency dependence of blocking temperature follows the Néel-Brown model [23]:

$$\tau = \tau_0 \exp\left(\frac{KV}{k_B T_B}\right), \tag{1}$$

where τ is related to measuring frequency ($\tau = 1/f$) and τ_0 is related to the jump attempt frequency of the magnetic moment of nanoparticle between the opposite directions of the magnetization easy axis. For SPM systems, τ_0 is in the range of 10^{-9}–10^{-13} s. Blocking temperature is the one that the thermal energy overcomes to anisotropy energy. When the energy of the potential barrier is comparable to thermal energy, the magnetization direction of the nanoparticles starts to fluctuate and goes through a rapid SPM relaxation. Above T_B the magnetization direction of nanoparticles can follow the direction of the applied field. Below the blocking temperature the thermal energy is less than the anisotropy energy; hence the direction of magnetization of each nanoparticle which may lie in the direction of easy axis is blocked. Since the nanoparticles and consequently their easy axes are randomly oriented, by decreasing the temperature, the total magnetic susceptibility is reduced. The linear plot of $\ln(f)$ versus the reciprocal of blocking temperature ($1/T_B$) is shown in Figure 5. The (KV/k_B) and τ_0 can be obtained from the slope and intercept of the plot. By fitting the experimental data we have found an unphysical small $\tau_0 \sim 1.26 \times 10^{-90}$ in comparison to the values of 10^{-9}–10^{-13} s for SPM systems. As expected, this result simply indicates that there exists strong interaction between nanoparticles of S3 sample. The interactions between nanoparticles affected the blocking/freezing temperature via modifying the energy barrier. On the other hand, the Vogel-Fulcher law describes the behavior of magnetically interacting (medium interaction) nanoparticles as follows [20]:

$$\tau = \tau_0 \exp\left(\frac{KV}{k_B (T_B - T_0)}\right). \tag{2}$$

In this model, T_0 is an effective temperature, representing the existence of the interaction between nanoparticles and τ_0 is a time-scale constant typically on the order of 10^{-9}–10^{-13} s. Fitting result with the Vogel-Fulcher law is given in Figure 6. According to Dormann et al. studies [20], the Vogel-Fulcher law is valid only if $T_0 \ll T_B$. In our work T_0 is 199 K, while the average value of T_B is 202 K. This point revealed that Vogel-Fulcher law cannot explain the behavior of the sample.

Two criteria have often been used to compare the frequency sensitivity of peak temperature in different samples and to distinguish between canonical spin glasses, other disordered magnetic compounds, where the freezing is progressive, and fine particles. They are given as [20]

$$c_1 = \left(\frac{\Delta T_f}{T_f \Delta(\log_{10} f)}\right), \qquad c_2 = \left(\frac{T_f - T_0}{T_f}\right), \tag{3}$$

where ΔT_f is the difference between T_f measured at the frequency $\Delta(\log_{10} f)$ interval. $\Delta T_f = T_f\,(f = 1000\,\text{Hz}) - T_f\,(f = 33\,\text{Hz})$ and T_f is the mean value of blocking/freezing temperature in the range of experimental frequencies and T_0 is the characteristic temperature of the Vogel-Fulcher law, (2). The value of c_1, which is independent of any model, represents the relative shift of blocking temperature per decade of frequency. The value of c_2 can be useful to compare the T_f variation between various systems. The experimental values of c_1 and c_2 depend on the interaction strength between magnetic nanoparticles. Dormann et al. distinguish three different types of dynamical behavior based on the values of c_1 and c_2: (1) for noninteracting particles $0.1 < c_1 < 0.13$ and $c_2 = 1$, (2) for weak interaction regime (inhomogeneous freezing) $0.03 < c_1 < 0.06$ and $0.3 < c_2 < 0.6$, and in the medium to strong interaction regime (homogeneous freezing) $0.005 < c_1 < 0.02$ and $0.07 < c_2 < 0.3$ [17]. Both c_1 and c_2 decrease with increasing the interactions between nanoparticles. The calculated values of c_1 and c_2 for our sample are 0.01 and 0.015, respectively. By comparing the c_1 and c_2 values, with values just given above, one can claim that there is a strong interaction between LSMO nanoparticles.

In the case of strong interaction between nanoparticles, magnetic nanoparticles indicate superspin glass behavior

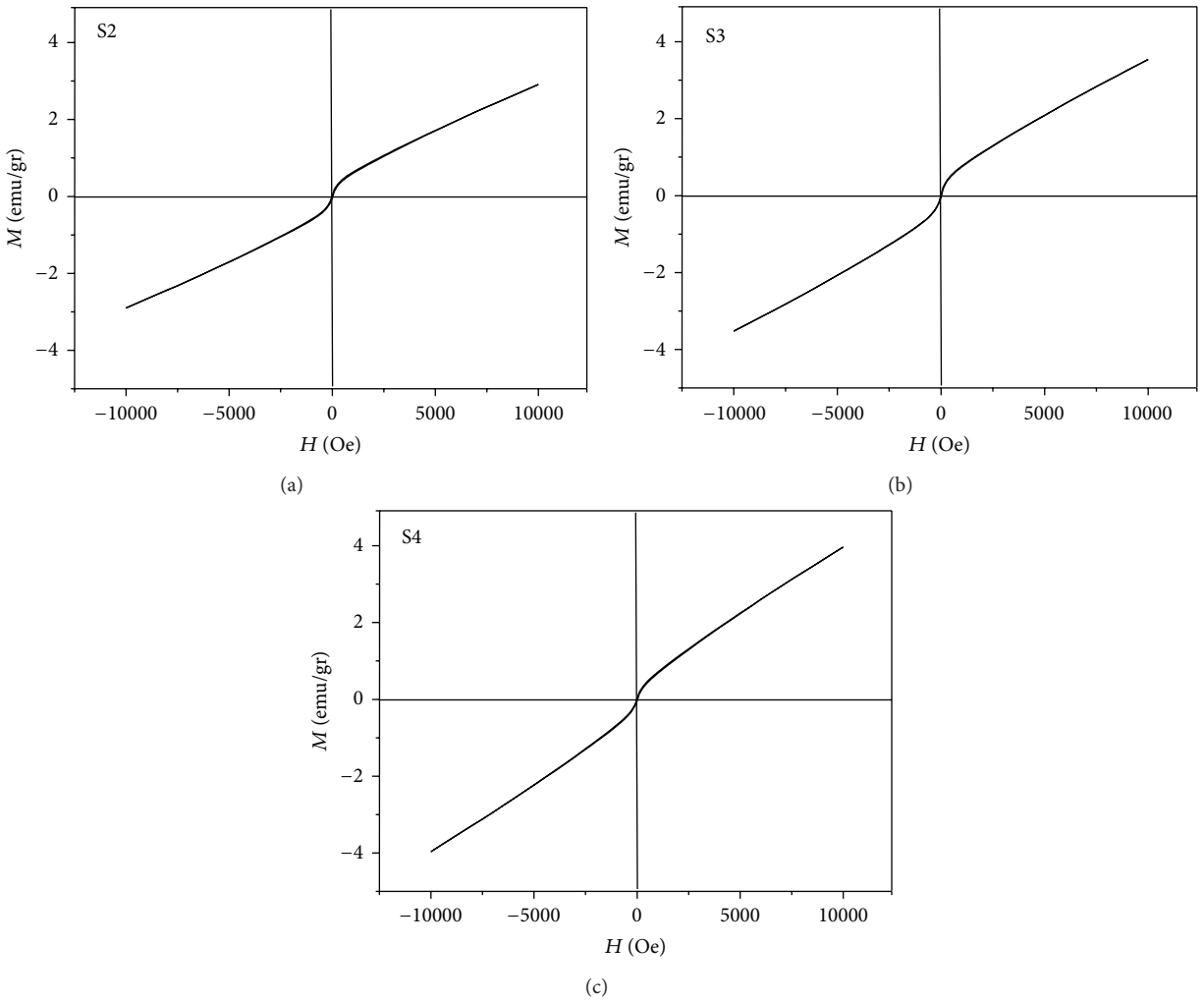

Figure 3: Room temperature magnetization versus magnetic field of the S2, S3, and S4 samples.

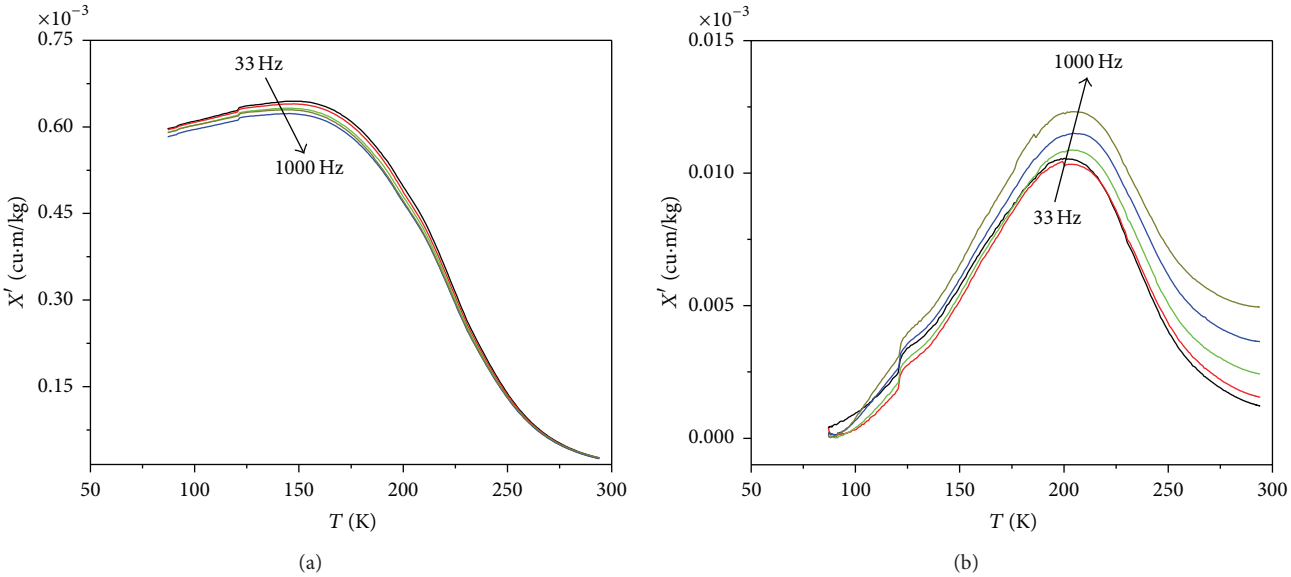

Figure 4: Frequency dependence of real and imaginary parts of ac susceptibility for sample S3, in frequencies of 33–1000 Hz and ac field of 10 Oe.

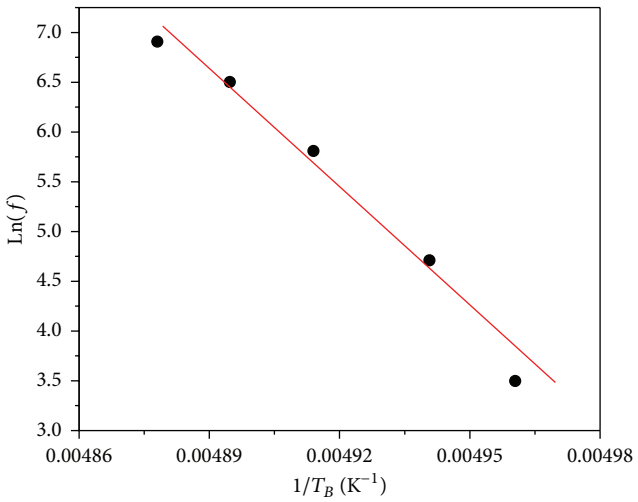

Figure 5: The best fits of ac magnetic susceptibility data for sample S3, using Néel-Brown model.

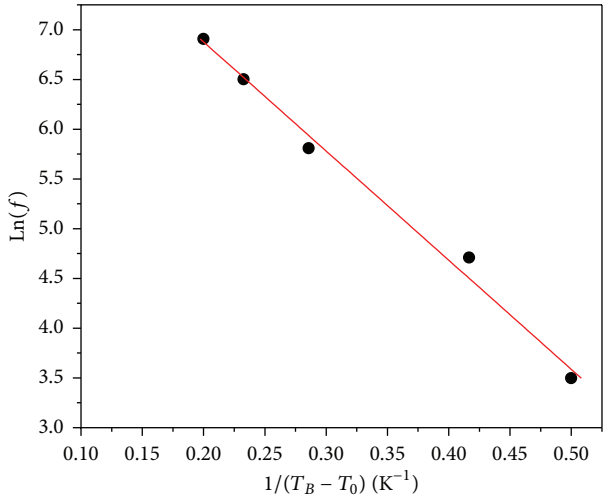

Figure 6: The best fits of ac magnetic susceptibility data for sample S3, using Vogel-Fulcher model.

[24]. The possibility of presence of a spinglass behavior was examined by the critical slowing down model [24] as follows:

$$\tau = \tau_0 \left(\frac{T_f}{T_g} - 1 \right)^{-z\upsilon}, \quad (4)$$

where T_f is the freezing temperature and T_g is the glass-transition temperature. The exponent depends on the law governing the phase transition, τ_0 is related to the relaxation time of the individual particle magnetic moment, υ is the critical exponent of correlation length, $\xi = (T_f/T_0 - 1)^{-\upsilon}$, and z relates τ and ξ as $\tau \sim \xi^z$. The parameter $z\upsilon$ as a dynamic critical exponent shows interactions strength and varies between 4 and 12 and τ_0 is in the range of 10^{-9}–10^{-13} s for frustrated three-dimensional systems such as spin glasses, reentrant spin glasses, and superspin glasses (SSG) [25, 26]. Figure 7 shows the best fits of ac magnetic susceptibility

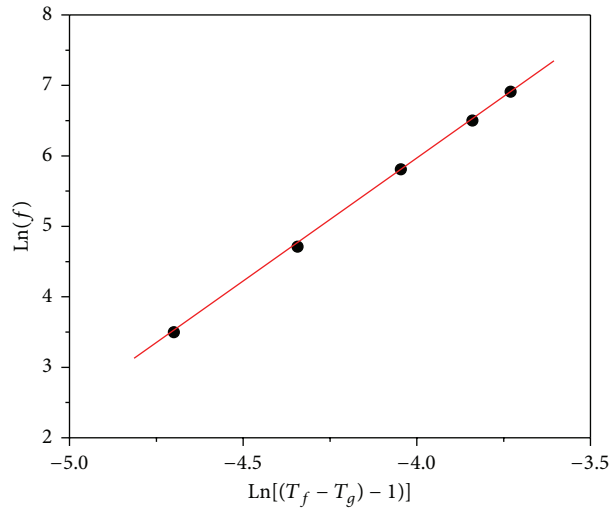

Figure 7: The best fits of ac magnetic susceptibility data for sample S3, using critical slowing down model.

data using the critical slowing down model. The obtained values of τ_0 and $z\upsilon$ are 4.17×10^{-11} and 4.8, respectively. Based on the calculated values of $z\upsilon$ and τ_0, the behavior of our sample is consistent with those expected for spin glass systems and could suggest the existence of a phase transition to a SSG state below the peak temperature. This type of SSG-like behavior has been reported elsewhere for different samples. For example, Fiorani et al. reported the values of $\tau_0 \sim 10^{-11}$ and $z\upsilon = 7.6$ for interacting nanoparticles of γ-Fe_2O_3 [27]. Also the SSG-like behavior has been reported in oleic acid-coated $Mn_{0.5}Zn_{0.5}Fe_2O_4$ ferrite nanoparticles by Parekh and Upadhyay [28].

4. Conclusions

The $La_{0.9}Sr_{0.1}MnO_3$ (LSMO) manganite nanoparticles could be synthesized successfully in nanocrystalline form by the microwave-assisted sol-gel auto-combustion method. The estimated negligible coercivity and remanent magnetization indicate superparamagnetic behavior for these nanoparticle samples. Spin dynamics analysis, using ac magnetic susceptibility measurements, showed that these nanoparticles have superspin glass behavior with strongly interacting superspins.

Conflict of Interests

The authors declare that there is no conflict of interests regarding the publication of this paper.

Acknowledgment

The authors would like to thank the Payame Noor University for supporting this work.

References

[1] M. Todorovic, S. Schuttz, J. Wong, and A. Scherer, "Writing and reading of single magnetic domain per bit perpendicular patterned media," *Applied Physics Letters*, vol. 74, p. 2516, 1999.

[2] T. D. Schladt, K. Schneider, H. Schild, and W. Tremel, "Synthesis and bio-functionalization of magnetic nanoparticles for medical diagnosis and treatment," *Dalton Transactions*, vol. 40, no. 24, pp. 6315–6343, 2011.

[3] L. Zhang and T. J. Webster, "Nanotechnology and nanomaterials: promises for improved tissue regeneration," *Nano Today*, vol. 4, no. 1, pp. 66–80, 2009.

[4] S. Jin, T. H. Tiefel, M. McCormack, R. A. Fastnacht, R. Ramesh, and L. H. Chen, "Thousandfold change in resistivity in magnetoresistive La-Ca-Mn-O films," *Science*, vol. 264, no. 5157, pp. 413–415, 1994.

[5] A. Asamitsu, Y. Moritomo, Y. Tomioka, T. Arima, and Y. Tokura, "A structural phase transition induced by an external magnetic field," *Nature*, vol. 373, no. 6513, pp. 407–409, 1995.

[6] Y. Tokura, *Colossal Magnetoresistive Oxides*, Gordon and Breach Science, Singapor, 2000.

[7] C. Zener, "Interaction between the d-shells in the transition metals. II. Ferromagnetic compounds of manganese with perovskite structure," *Physical Review B*, vol. 82, no. 3, pp. 403–405, 1951.

[8] A. J. Millis and P. B. Shramin, "Double exchange alone does not explain the resistivity of $La_{1-x}Sr_xMnO_3$," *Physical Review Letters*, vol. 74, no. 25, pp. 5144–5147, 1995.

[9] R. D. Sánchez, J. Rivas, C. Vázquez et al., "Giant magnetoresistance in fine particle of $La_{0.67}Ca_{0.33}MnO_3$ synthesized at low temperatures," *Applied Physics Letters*, vol. 68, p. 134, 1996.

[10] N. Zhang, W. Ding, W. Zhong, D. Xing, and Y. Du, "Tunnel-type giant magnetoresistance in the granular perovskite $La_{0.85}Sr_{0.15}MnO_3$," *Physical Review B*, vol. 56, p. 8138, 1997.

[11] K. Wang, W. Song, T. Yu, B. Zhao, M. Pu, and Y. Sun, "Colossal magnetoresistance in fine particle of layered-perovskite $La_{2-2x}Ca_{2+2x}Mn_2O_7$ (x = 0.3) synthesized at low temperatures," *Physica Status Solidi A*, vol. 171, no. 2, pp. 577–582, 1999.

[12] A. Rostamnejadi, H. Salamati, P. Kameli, and H. Ahmadvand, "Superparamagnetic behavior of $La_{0.67}Sr_{0.33}MnO_3$ nanoparticles prepared via sol-gel method," *Journal of Magnetism and Magnetic Materials*, vol. 321, no. 19, pp. 3126–3131, 2009.

[13] S. Daengsakul, C. Thomas, C. Mongkolkachit, and S. Maensiri, "Effects of crystallite size on magnetic properties of thermal-hydro decomposition prepared $La_{1-x}Sr_xMnO_3$ nanocrystalline powders," *Solid State Sciences*, vol. 14, no. 9, pp. 1306–1314, 2012.

[14] P. Kameli, H. Salamati, and A. Aezami, "Effect of particle size on the structural and magnetic properties of $la_{0.8}Sr_{0.2}MnO_3$," *Journal of Applied Physics*, vol. 100, no. 5, Article ID 053914, 2006.

[15] D. G. Kuberkar, R. R. Doshi, P. S. Solanki et al., "Grain morphology and size disorder effect on the transport and magnetotransport in sol-gel grown nanostructured manganites," *Applied Surface Science*, vol. 258, no. 22, pp. 9041–9046, 2012.

[16] A. Rostamnejadi, H. Salamati, and P. Kameli, "Magnetic properties of interacting $La_{0.67}Sr_{0.33}MnO_3$ nanoparticles," *Journal of Superconductivity and Novel Magnetism*, vol. 25, no. 4, pp. 1123–1132, 2012.

[17] J. L. Dormann, D. Fiorani, and E. Tronc, "On the models for interparticle interactions in nanoparticle assemblies: comparison with experimental results," *Journal of Magnetism and Magnetic Materials*, vol. 202, no. 1, pp. 251–267, 1999.

[18] J. Rodríguez-Carvajal, "Recent advances in magnetic structure determination by neutron powder diffraction," *Physica B*, vol. 192, no. 1-2, pp. 55–69, 1993.

[19] K. P. Shinde, S. S. Pawar, and S. H. Pawar, "Influence of annealing temperature on morphological and magnetic properties of $La_{0.9}Sr_{0.1}MnO_3$," *Applied Surface Science*, vol. 257, no. 23, pp. 9996–9999, 2011.

[20] J. L. Dormann, D. Fiorani, and E. Tronc, "Magnetic relaxation in fine-particle systems," *Advances in Chemical Physics*, vol. 98, pp. 283–494, 1997.

[21] M. Suzuki, S. I. Fullem, I. S. Suzuki, L. Wang, and C. Zhong, "Observation of superspin-glass behavior in Fe_3O_4 nanoparticles," *Physical Review B*, vol. 79, no. 2, Article ID 024418, 7 pages, 2009.

[22] B. Aslibeiki, P. Kameli, I. Manouchehri, and H. Salamati, "Strongly interacting superspins in Fe_3O_4 nanoparticles," *Current Applied Physics*, vol. 12, no. 3, pp. 812–816, 2012.

[23] M. Tadić, V. Kusigerski, D. Marković, M. Panjan, I. Milošević, and V. Spasojević, "Highly crystalline superparamagnetic iron oxide nanoparticles (SPION) in a silica matrix," *Journal of Alloys and Compounds*, vol. 525, pp. 28–33, 2012.

[24] B. Aslibeiki, P. Kameli, H. Salamati, M. Eshraghi, and T. Tahmasebi, "Superspin glass state in $MnFe_2O_4$ nanoparticles," *Journal of Magnetism and Magnetic Materials*, vol. 322, no. 19, pp. 2929–2934, 2010.

[25] J. Mydosh, "Disordered magnetism and spin glasses," *Journal of Magnetism and Magnetic Materials*, vol. 157-158, pp. 606–610, 1996.

[26] M. Thakur, M. Patra, S. Majumdar, and S. Giri, "Coexistence of superparamagnetic and superspin glass behaviors in $Co_{50}Ni_{50}$ nanoparticles embedded in the amorphous SiO_2 host," *Journal of Applied Physics*, vol. 105, no. 7, Article ID 073905, 2009.

[27] D. Fiorani, A. M. Testa, F. Lucari, F. D'Orazio, and H. Romero, "Magnetic properties of maghemite nanoparticle systems: surface anisotropy and interparticle interaction effects," *Physica B: Condensed Matter*, vol. 320, no. 1–4, pp. 122–126, 2002.

[28] K. Parekh and R. V. Upadhyay, "Static and dynamic magnetic properties of monodispersed $Mn_{0.5}Zn_{0.5}Fe_2O_4$ nanomagnetic particles," *Journal of Applied Physics*, vol. 107, no. 5, Article ID 053907, 2010.